

## Bearing Fault Diagnosis Based on Improved Pseudo Fourth Order Moment

Zihan Wang, Jian Wang and Yongjian Sun\*

Electrical Engineering, University of Jinan, Jinan, Shandong, China

\*Corresponding author: Yongjian Sun, Electrical Engineering, University of Jinan, Jinan, Shandong, China. Email: sunyongjian2006@163.com

Citation: Wang, Z., Wang, J., & Sun, Y. (2023). Bearing Fault Diagnosis Based on Improved Pseudo Fourth Order Moment. *J Artif Intell Mach Learn & Data Sci*, 1(1), 10-20.

Received: 30 December, 2022; Accepted: 07 February, 2023; Published: 09 February, 2023

Copyright: © 2023 Sun, Y., et al., This is an open-access article distributed under the terms of the Creative Commons Attribution License, which permits unrestricted use, distribution, and reproduction in any medium, provided the original author and source are credited.

### ABSTRACT

In this paper, a new method of bearing fault diagnosis based on ensemble empirical mode decomposition (EEMD) and anchor point is advanced and verified. EEMD decomposition of vibration signals to rolling bearings on different working conditions, the pseudo-fourth-order moment (PFOM) of the decomposed signals calculated. Based on the definition of anchor point, a novel fault feature fitting anchor value proposed. Newton interpolation is adopted to fit the PFOM, and the anchor point is brought into the fitting function to get the anchor point fitting value. A large amount of data was obtained through many experiments, and the range of anchor fitting values under normal and five kinds of faults were determined. The anchor fitting value as the feature used to classify six working conditions. Taking the fitting value of the anchor point as the fault feature, the training data is selected and put into the extreme learning machine (ELM), and different working conditions are classified. Then take the test data and put it into the ELM model based on the training data for diagnosis, and the final classification accuracy reaches 97.5%. Finally, three comparative experiments shows that the present method are effective against the field of bearing fault diagnosis.

**Keywords:** Ensemble Empirical Mode Decomposition, Pseudo-fourth-order Moment, Anchor Point, Extreme Learning Machine.

### Introduction

In most large-scale mechanical equipment, rolling bearing is a part of it, which plays a key role. Whether the rolling bearing can function safely and trouble-free, to a great extent, relates to the operation of the whole equipment, so it is an essential step to make an accurate diagnosis of the rolling bearing [1]. With the continuous development of industrial equipment, the structure of mechanical equipment in all walks of life has become more and more complex, and the relationship between various parts has become closer and closer [2]. Therefore, if the rolling bearing is damaged, it will lead to problems in the operation of the whole industrial equipment, thus affecting the normal operation of the whole industrial equipment, possibly endangering people's lives and leading to irreparable consequences [3]. In early years, the fault diagnosis of the rolling bearing depends on manpower, so the early faults in the bearing cannot be found in time. Fortunately, the fault diagnosis of rolling bearings keeps pace with the times and develops with the progress of science and technology.

The vibration signal is the easiest to obtain, which can reflect the data of bearing state [4]. But the vibration signal of the rolling bearing is often influenced by the coupling of various vibration propagation paths, and the background noise and interference signal of the vibration signal is strong, which makes it hard for the traditional methods to produce results [5]. In the current field, many nonlinear and non-stationary signal processing methods are used [6]. Such as, Resonance-based Sparse Signal Decomposition (RSSD) [7], Wavelet Transform (WT) [8], empirical mode decomposition (EMD) [9]. Variational Modal Decomposition (VMD) [10], filters the original signal, decomposes the dominant frequency signals to the set of AM/FM signals, and assumes that the limited bandwidth of each mode has a center frequency so that the sum of estimated bandwidths of each mode is minimized, thus realizing the adaptive decomposition of the signal. CEEMD [11] is an improvement of empirical mode decomposition (EMD) and integrated empirical mode decomposition (EEMD), which can completely decompose signals. CEEMD adds a group of white noises with opposite positive and negative to the original

signal, which can not only suppress the mode alias of EMD but also keep the residual noise at a low level all the time and then ignored. However, CEEMD has a large amount of calculations, and when processing a large amount of data, the program runs too long, which affects the efficiency.

Although vibration diagnosis technology can diagnose some typical faults of rolling bearings, with the increasingly complex structure of rolling bearings, the positions and forms of faults are gradually diversified, making it difficult to diagnose them accurately [12]. With the development of artificial intelligence technology, many machines learning methods has been applied to fault diagnosis of rolling bearings. Such as deep learning [13], Enfigram [14], non-parallel least squares support matrix machine (NPLSSMM) [15]. Hu et al. apply deep learning [16] to fault diagnosis of rolling bearing, and explored the feasibility of stack noise reduction white cod at fault diagnosis of rolling bearing. This method analyzed and discussed the influence of different hidden layer combinations on identification rate and studied the feasibility of realizing intelligent identification of bearing faults by stack noise reduction self-coding method. Zheng et al.[17] found an improved multi-scale permutation entropy (MPE) method, called generalized compound multi-scale permutation entropy (GCMPE), which solved the shortcomings of rough grain in MPE and improved the accuracy. Pang et al. propose an ensemble learning diagnosis method [18]. This method combines fast denoising with ELM, which improves the training speed of ELM, and has better learning ability when learning highly abstract features. It solves the problem that the domain drift caused by working condition fluctuation or noise will significantly reduce the diagnostic performance of existing deep learning methods. Hou et al.[19] find a novel method based on sparse representation theory with high accuracy. It is inspired by the traditional K-SVD based de-noising method and can penetrate into the underlying structure of the signal. The coefficients are globally optimized based on an (l1)-regularized least square problem solving method, which can locate the impulse coordinates more accurately compared with orthonormal matching pursuit (OMP) applied in the traditional K-SVD.

As a commonly used mechanical rotating component, rolling bearings are mainly composed of four parts: inner ring, outer ring, ball and cage [20]. From the simulation and the actual diagram of Figure 1, we can see the four components of a rolling bearing. The outer ring is installed in the bearing seat hole and generally does not rotate. The inner ring is mounted on the journal and rotates with the shaft. Rolling element is the core element of rolling bearing and plays a rolling role. The cage rollers are evenly spaced to avoid friction with each other.

The structure of the rest of this paper is as follows: The second section introduces the feature reconstruction of bearing failure. The third section introduces the diagnosis scheme and the specific experimental flow. The fourth section starts the simulation experiment and gives the corresponding data. In the fifth section, a comparative experiment was carried out. Finally, the conclusion is given.

## Feature reconstruction of bearing fault

### Data standardization

Through the standardized processing of data, the original data can be converted into index evaluation values without dimensions, and each index value is in the same order of magnitude, so it can be comprehensively evaluated and analyzed. If the original data are directly used for analysis without processing, the higher

values will have a greater impact on the analysis, while the lower values will have a smaller impact, resulting in erroneous analysis [22]. After processing, it can be better analyzed and judged more effectively. The extracted rolling bearing vibration data is standardized by eq1:

$$x^* = \frac{x - x_{min}}{x_{max} - x_{min}} \quad (1)$$

where,  $x^*$  is the standardized processed data,  $x$  is the original data,  $x_{max}$  is the maximum value in the original data,  $x_{min}$  is the minimum value in the original data.

By readjusting the value of each dimension of data, the final data vector falls within the [0,1] interval. This normalization method is more suitable for the situation where the rolling bearing data are relatively concentrated. The maximum and minimum values of little change, simple and stable.

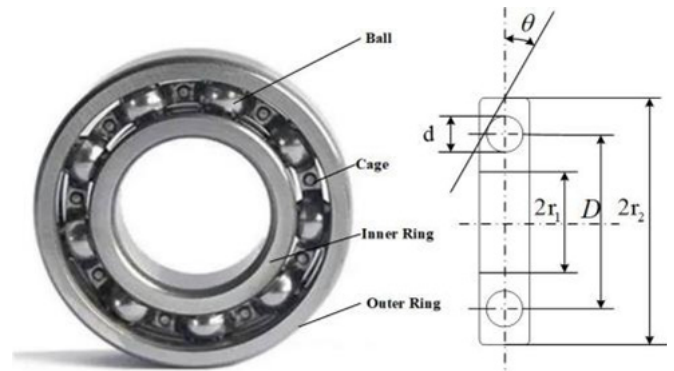


Figure 1: Rolling bearing structure

### EEMD

Ensemble empirical mode decomposition (EEMD) is a classical noise-assisted signal analysis method [23]. By adding Gaussian white noise with a given amplitude to the original signal, EMD and averaging are carried out many times to solve the problem of modal aliasing. In this method, the statistical characteristics of uniform Gaussian white noise frequency distribution is used to change the distribution characteristics of extreme points of the original signal so that the signal has continuity in different characteristic scales and the error of envelope fitting of upper and lower extreme points is avoided [24].

The realization can be summarized as follows:

- (1) adding Gaussian white noise sequence with amplitude coefficient  $k$   $m$  times to original signal  $x(t)$  to obtain  $x_i(t)$  ( $i = 1, 2, \dots, M$ ).
- (2) The signals  $x_i(t)$  obtained in step (1) are decomposed by EMD to obtain  $N$  IMF components  $c_{ij}(t)$  ( $j = 1, 2, \dots, N$ ) and a residual component  $s_i(t)$ .

$$x_i(t) = \sum_{j=1}^N c_{ij}(t) + s_i(t) \quad (2)$$

where,  $c_{ij}(t)$  is the  $j$  IMF component of the  $i$ th decomposition,  $s_i(t)$  is the residual component of the  $i$ th decomposition.

- (3) Average the decomposed IMF component  $c_{ij}(t)$  and residual component  $s_i(t)$ , eliminate the influence of noise on IMF component, and get

$$c_j(t) = \frac{1}{M} \sum_{i=1}^M c_{ij}(t) \quad (3)$$

$$s(t) = \frac{1}{M} \sum_{i=1}^M s_i(t) \quad (4)$$

Therefore, the original signal  $x(t)$  is decomposed into  $N$  IMF components  $c_j(t)$  ( $J = 1, 2, \dots, N$ ) and a residual component  $s(t)$ .

$$x(t) = \sum_{j=1}^N c_j(t) + s(t) \quad (5)$$

### Pseudo fourth-order Moment (PFOM)

Traditional fourth-order moment calculation is tedious, which takes up a lot of resources and computing power and consumes a lot of time when calculating on the computer, which seriously affects the efficiency. Moreover, the requirements of multi-computers are higher, and ordinary computers may not be competent. For this reason, PFOM is designed to weaken the orthogonality condition, and the orthogonality of the signal obtained by EEMD decomposition is lost, so PFOM can be obtained by a simple calculation. The method is as follows:

$$k = \frac{a_1^4 + a_2^4 + \dots + a_n^4}{l(n*\eta)} \quad (6)$$

where,  $K$  is PFOM,  $a_n$  is the data,  $l = \frac{1}{n}$ .

### Newton interpolation method

When we only know the position of the function at some nodes but don't know the specific expression of the function, we can use the algebraic interpolation method to give the approximate form of the function. In this paper, the Newton interpolation method is used to get the approximate function of fitting. The specific method is as follows:

Let the function  $f(x)$  be known that its  $n+1$  interpolation nodes are  $(x_i, y_i)$ ,  $i = 0, 1, 2, \dots, n$ , we define:

The zero-order difference quotient of  $f(x)$  in is  $f(x_i)$ ;

The first-order quotient of  $f(x)$  at points and is  $f(x_i, x_j) = \frac{f(x_j) - f(x_i)}{x_j - x_i}$ .

The second-order quotient of  $f(x)$  at points  $x_i, x_j$  and  $x_k$  is  $f(x_i, x_j, x_k) = \frac{f(x_j, x_k) - f(x_i, x_j)}{x_k - x_i}$ .

Generally, the  $k$ -order quotient of  $f(x)$  at point  $x_0, x_1, \dots, x_k$  is:

$$f(x_0, x_1, \dots, x_k) = \frac{f(x_1, x_2, \dots, x_k) - f(x_0, x_1, \dots, x_{k-1})}{x_k - x_0} \quad (7)$$

After the difference quotient is obtained, Newton interpolation method can be used for fitting. Calculate the difference quotient of  $f(x)$  and bring it into the formula.

$$f(x) = f(x_0) + (x - x_0)f(x_0, x_1) + (x - x_0)(x - x_1)f(x_0, x_1, x_2) + \dots + (x - x_0)(x - x_1) \dots (x - x_{n-1})f(x_0, x_1, \dots, x_{n-1}) \quad (8)$$

### Anchor point

After the standardized rolling bearing vibration signal data is decomposed by EEMD, five layers of signals are obtained. Calculate the PFOM of the obtained signal. A fitting function can be obtained by fitting the obtained PFOM with Newton interpolation method. The fitting function of different working conditions is different. In order to extract features conveniently, the point with the greatest discrimination of the function image

is set as the anchor point.

Different anchor points corresponding to different results affect the extracted fault characteristics. Therefore, it is necessary to find the best anchor point.

In order to find the anchor point, which is the most distinguished point of fitting function of six working conditions, a formula is derived:

$$k(x, x') = e^{-\frac{\|x-x'\|^2}{2\sigma^2}} \quad (9)$$

where, is the degree of discrimination, with a maximum of 1 and a minimum of 0, is the anchor point, is variable and  $\sigma$  is bandwidth,  $\sigma = 0.5$ .

After a lot of calculations, when the anchor point is between 1.0 and 1.4, the accuracy of fault diagnosis is higher, and the fault features have better discrimination.

### Extreme learning machine

In this paper, extreme learning machine is used as classifier. Compared with support vector machine (SVM), which is widely used in the field of fault diagnosis, extreme learning machine (ELM) has better multi-classification effect and faster speed. Through the classifier of extreme learning machine [25] a fault diagnosis scheme for rolling bearings is designed. ELM algorithm is as follows:

$$\sum_{i=1}^M \beta_i g(w_i x_i + b_i) = o_j, \quad j = 1, 2, \dots, n \quad (10)$$

- The weight  $w_i$  and the hidden layer deviation  $b_i$  are initialized and kept constant.

- The matrix  $H$  of the hidden layer output is calculated.

$$H(w_1, \dots, w_L, b_1, \dots, b_L, x_1, \dots, x_L) = \begin{bmatrix} g(w_1 x_1 + b_1) & \dots & g(w_L x_1 + b_L) \\ \vdots & \ddots & \vdots \\ g(w_1 x_N + b_1) & \dots & g(w_L x_N + b_L) \end{bmatrix} \quad (11)$$

- Calculation  $\beta$ .

$$H\beta = T, \beta = \begin{bmatrix} \beta_1^T \\ \vdots \\ \beta_L^T \end{bmatrix}, T = \begin{bmatrix} T_1^T \\ \vdots \\ T_N^T \end{bmatrix} \quad (12)$$

- Put the data into the extreme learning machine.

### Range division

Ten thousand data extracted from six working conditions respectively, and the data were standardized and then decomposed by EEMD. Take the first five layers of decomposed data and calculate the pseudo-fourth moment. Newton interpolation method is used to fit the pseudo-fourth moment, and the fitting function is obtained. Bring the anchor point into the fitting function and get the fitting value of the anchor point. Repeat the above steps many times to determine the anchorage fitting value range of six working conditions. The fitting numerical range of anchor point in normal working conditions is 0.08644~0.13987. The fitting numerical range of fault 1 anchor point is 1.93677~3.01581. The fitting numerical range of anchor point of rolling body fault in normal working condition is 1.22515~2.41464. The fitting numerical range of anchor point of outer ring fault 1 under normal working condition is 2.50308~13.14295. The fitting numerical range of fault 2 anchor point is 4.39316~29.52875. The fitting numerical range of anchor

point of outer ring fault 2 under normal working condition is 1.03532~1.74344. After the range of anchor fitting value is determined, it can be used to distinguish six working conditions. This result is correct when the fitting values of anchor points in six working conditions are within the corresponding range. If the anchor fitting value is not in the corresponding range, the result will be wrong.

**Diagnostic scheme**

In the traditional method, the pseudo-fourth moment is directly taken as the characteristics of rolling bearings under different working conditions. But this method actually ignores a lot of information contained in the pseudo-fourth-order moment. In order to obtain more fault information and better realize fault diagnosis of rolling bearings, this paper combines pseudo-fourth-moment with interpolation fitting. In order to obtain the best diagnosis result, the concept of anchor point is put forward. By introducing the anchor point into the fitting curve, the fitting value of the anchor point is taken as the fault feature of the rolling bearing. This promotion greatly expands the application of pseudo-fourth-moment in fault diagnosis.

The fault diagnosis program of rolling bearing based on anchor fitting value is developed as follows:

1. In the data set of each working condition of rolling bearing, the same number of continuous data are randomly selected as experimental data.
2. The experimental data of different working conditions are processed by EEMD, and N-layer IMFs is obtained.
3. Calculate the PFOM of each IMF layer, that is,  $k_n, n=1,2,\dots, m$ .  $k_n$  is the PFOM of the n-th IMF layer.
4. Coordinate points (n,  $k_n$ ) are composed of layers n and  $k_n$ . The coordinate points  $(1, k_1), (2, k_2), \dots, (m, k_m)$  are fitted by Newton interpolation method, and fitting functions are obtained.
5. According to the derived formula, the best anchor point is introduced. And the anchor point is brought into the fitting function to calculate the fitting value of the anchor point.
6. After many experiments, the fitting range of anchor point under six working conditions of rolling bearing is divided.
7. Through the extreme learning machine, the final classifier test is carried out and the correct rate is calculated.

As shown in Figure 2.

**Simulation Experiment**

The CWRU vibration data set is used in this paper. The following Figure 3 shows the experimental device for collecting CWRU vibration data set. The data used in this paper are as follows. The normal working condition is the data at the speed of 1750 rpm. Fault 1 of inner ring, fault of rolling element and fault 1 of outer ring are the data when the rotating speed is 1750 rpm, and the fault diameter is 0.1778 mm. Fault 2 of the inner ring and fault 2 of the outer ring are the data when the rotating speed is 1797 rpm, and the fault diameter is 0.3556 mm.

The specific steps of simulation are shown in Figure 4.

The simulation is divided into three steps. The first step is to preprocess the basic data of rolling bearings, display the time domain images of vibration signals of each rolling bearing under six working conditions, and normalize the data. The second step

is feature extraction, including EEMD decomposition, pseudo-fourth-order moment calculation, anchor fitting value extraction, and anchor fitting value range establishment. The third step is to use ELM classifier for testing.

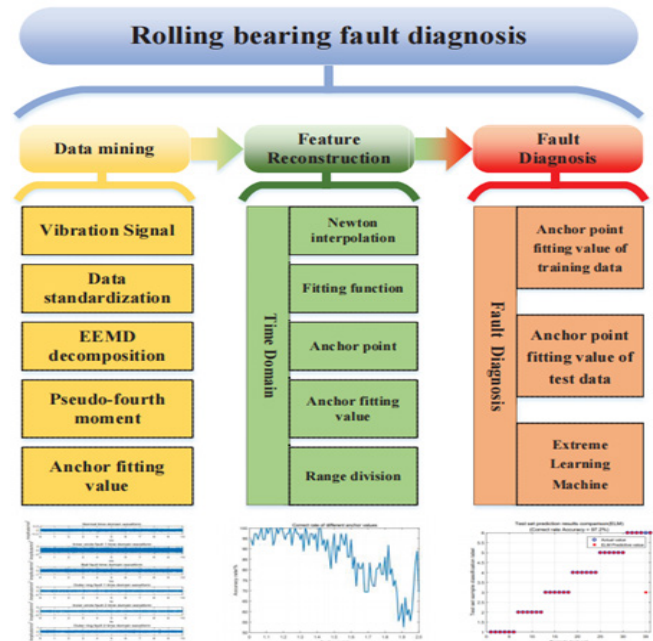


Figure 2: Design scheme of experiment.

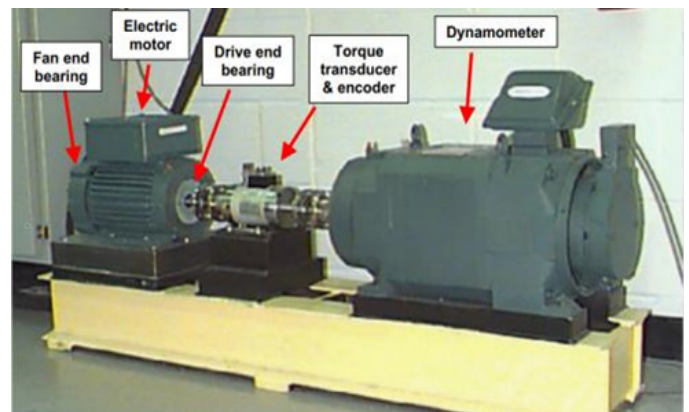


Figure 3: CWRU bearing experimental device.

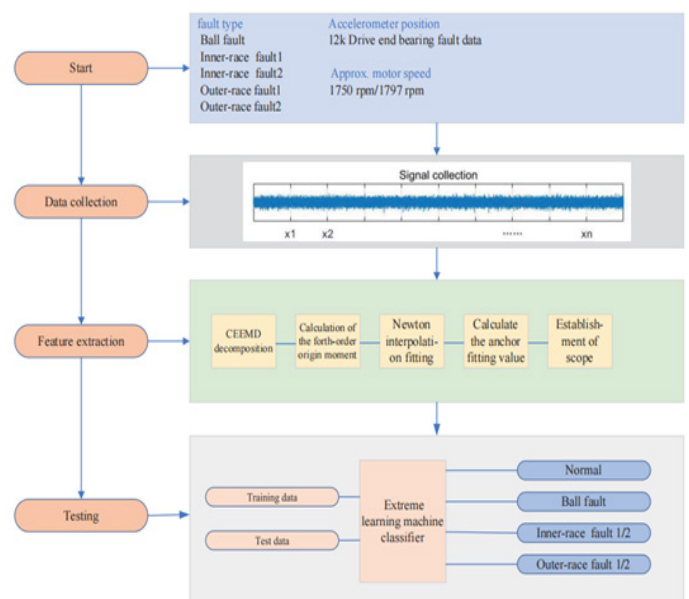


Figure 4: Design scheme of experiment.

Time-domain images of vibration signals of rolling bearings in six working conditions are shown in Figure 5.

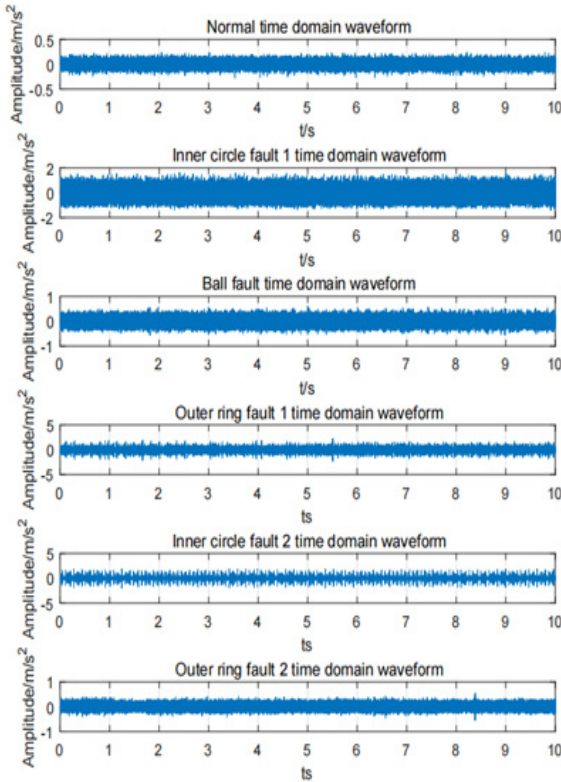


Figure 5: Vibration signals in time domain.

From the time-domain signal images of rolling bearings, it can be seen that the vibration signals produced by bearings under different working conditions are different, but there are differences, but they are not obvious. Only by the vibration signal neither the human eye nor the computer can make an accurate judgment, which has a great error. Therefore, it is necessary to dig deeper into the vibration signal data to find out the characteristics of each working condition. There are many ways to deal with vibration information, but EEMD is undoubtedly a good choice. EEMD solves the problems of modal aliasing in EMD, and at the same time, it has both accuracy and rapidity.

The EEMD can decompose the signal into multiple layers, show the characteristics of the original data at different times, and mine the data well. Considering the requirements of computation and running time, only the first five layers of inherent modal components (IMF) are selected in this paper. The time-domain signal is decomposed by EEMD, as shown in Figure 6 to Figure 11.

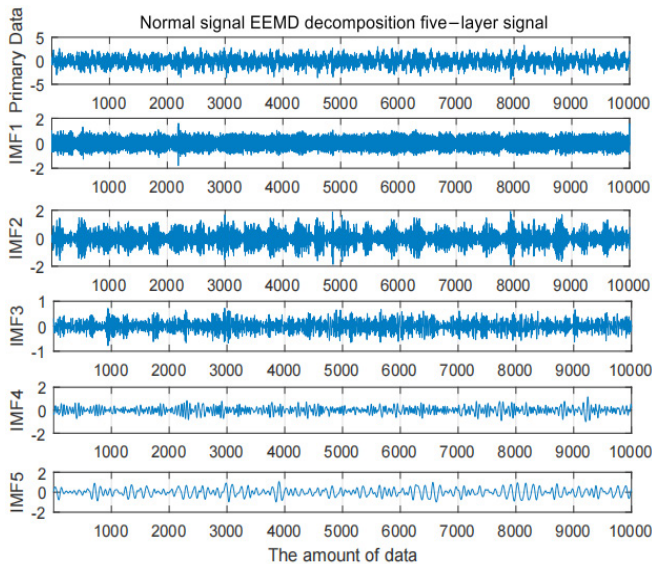


Figure 6: Normal signal EEMD.

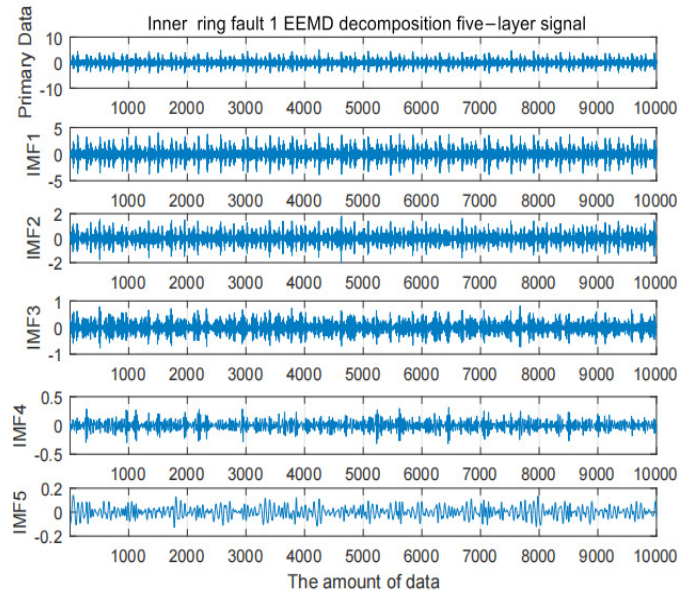


Figure 7: Inner ring fault 1 EEMD.

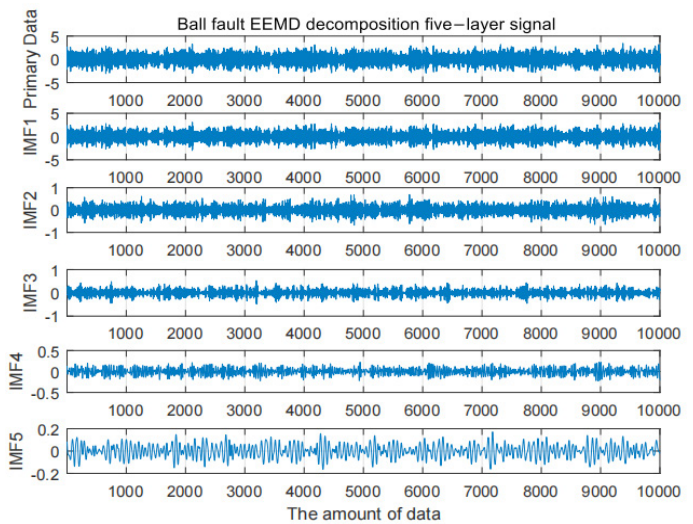


Figure 8: Ball fault EEMD.

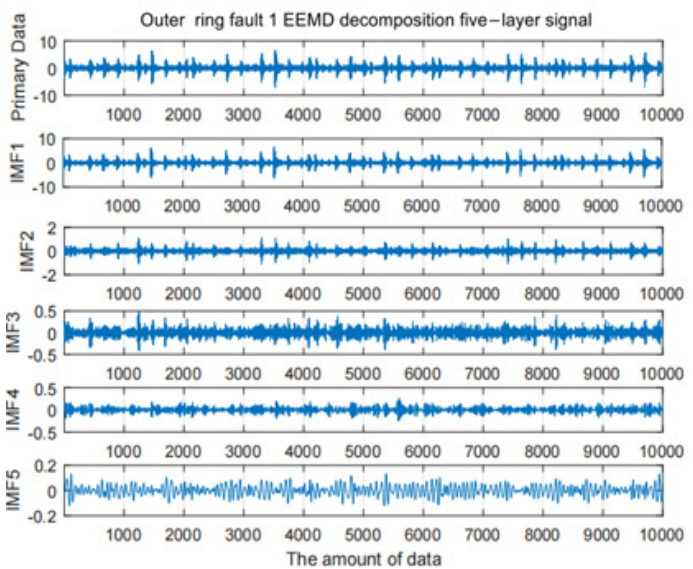


Figure 9: Outer ring fault 1 EEMD.

After EEMD decomposition, the original data has changed a lot, and the available information has increased. At this time, if the obtained data is input into the extreme learning machine, a good result cannot be obtained. But it is still not enough for the computer to easily classify the six working conditions of rolling bearings. If the fault diagnosis of rolling bearing can't be

completed, it still needs deeper extraction. Therefore, the PFOM is introduced in this paper. Based on the obtained five-layer IMF, the PFOM is calculated. The experimental data selected in this paper are continuous data with a length of 6000 in the rolling bearing data set of Western Reserve University. The selection of these data is random. The experimental data is decomposed by EEMD to obtain 5-layer IMF. Calculate the PFOM of the IMF in the first to fifth layers under each working condition. Table 1 to Table 6 summarizes the results of PFOM calculated six times with different experimental data under various working conditions.

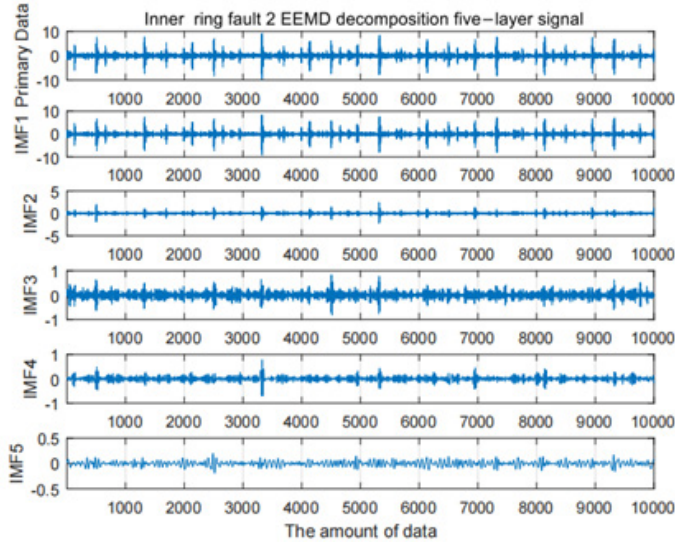


Figure 10: Inner ring fault 2 EEMD.

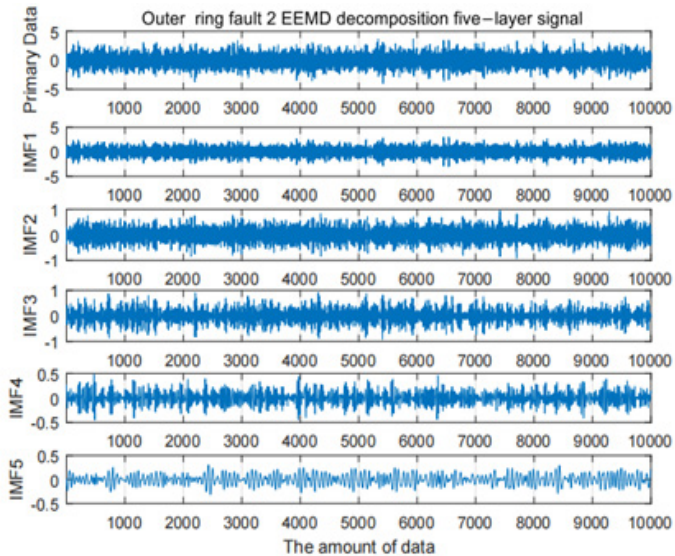


Figure 11: Outer ring fault 2 EEMD.

Table 1: PFOM in normal condition

	First layer signal	Second layer signal	Third layer signal	Fourth layer signal	Fifth layer signal
1	0.104890	0.234231	0.003717	0.017001	0.051791
2	0.061546	0.175258	0.009652	0.014929	0.168248
3	0.062340	0.165549	0.007364	0.021841	0.055907
4	0.148990	0.168241	0.006728	0.014879	0.065593
5	0.080645	0.206833	0.015108	0.146216	0.041683
6	0.092859	0.213619	0.008211	0.016863	0.033380

From the tables, we can see that PFOM under various working conditions is unstable and there is a certain intersection. That is, parts that contain or intersect with each other. If this feature is used for fault diagnosis, it will produce great errors and make wrong

judgments. It is still necessary to continue to extract features to get the diagnostic accuracy. In this paper, a brand-new method is created to further extract the fault characteristics of rolling bearings, that is, anchor point method. After the standardized rolling bearing vibration signal data is decomposed by EEMD, five layers of signals are obtained. Calculate the PFOM of the obtained signal. A fitting function can be obtained by fitting the obtained PFOM with Newton interpolation method. Coordinate points (n,) are composed of layers n and . The coordinate points (1, ), (2, ), ..., (5, ) are fitted by Newton interpolation method, and fitting functions are obtained. According to the derived formula, the best anchor point is introduced. The fitting function of different working conditions is different. In order to extract features conveniently, the point with the greatest discrimination of the function image is set as the anchor point. Different anchor points corresponding to different results affect the extracted fault characteristics. For this reason, each group of data obtained is fitted by Newton interpolation method, and a fitting function can be obtained. The fitting function is different under different working conditions. In order to extract features conveniently, I will define the point with the largest division in the function image as the anchor point. See eq9 for the selection of anchor points. And the anchor point is brought into the fitting function to calculate the fitting value of the anchor point. By bringing the anchor point into the fitting function, the fitting value of the anchor point can be obtained. Based on the fitting value of anchor point, the fault diagnosis of rolling bearing can be carried out. When the anchor point is between 1.0 and 1.4, the greater the discrimination of the fitting value of the anchor point as a feature, and the higher the accuracy of distinguishing various working conditions of the bearing.

Table 2: PFOM in inner ring fault 1.

	First layer signal	Second layer signal	Third layer signal	Fourth layer signal	Fifth layer signal
1	2.968791	0.105541	0.007305	0.000075	0.000007
2	3.112328	0.098536	0.003823	0.000261	0.000017
3	3.163065	0.125855	0.007231	0.000072	0.000015
4	3.548760	0.088502	0.008892	0.000181	0.000008
5	3.403726	0.139743	0.011422	0.000097	0.000014
6	3.274510	0.110665	0.009346	0.000269	0.000003

Table 3: PFOM in ball fault.

	First layer signal	Second layer signal	Third layer signal	Fourth layer signal	Fifth layer signal
1	2.275080	0.001754	0.001254	0.000119	0.000021
2	2.066753	0.003036	0.001088	0.000400	0.000019
3	2.225558	0.004007	0.001393	0.000078	0.000026
4	2.222781	0.002185	0.000981	0.000085	0.000037
5	2.269499	0.003786	0.001056	0.000166	0.000045
6	2.149660	0.002737	0.001655	0.000122	0.000034

Table 4: PFOM in outer ring fault 1.

	First layer signal	Second layer signal	Third layer signal	Fourth layer signal	Fifth layer signal
1	9.101338	0.003941	0.000289	0.000058	0.000006
2	9.262672	0.004673	0.000176	0.000056	0.000003
3	5.073220	0.006222	0.000197	0.000069	0.000009
4	9.745454	0.007644	0.000171	0.000039	0.000003
5	6.283764	0.014097	0.000413	0.000080	0.000014
6	8.213266	0.003960	0.000218	0.000100	0.000017

**Table 5:** PFOM in inner ring fault 2.

	First layer signal	Second layer signal	Third layer signal	Fourth layer signal	Fifth layer signal
1	17.342949	0.019238	0.001560	0.000637	0.000010
2	12.370938	0.046163	0.001501	0.000409	0.000041
3	16.853678	0.018278	0.001784	0.001481	0.000027
4	14.748240	0.017147	0.001398	0.000410	0.000070
5	21.918791	0.025963	0.002539	0.000511	0.000018
6	15.646733	0.010551	0.002640	0.000660	0.000056

**Table 6:** PFOM in outer ring fault 2.

	First layer signal	Second layer signal	Third layer signal	Fourth layer signal	Fifth layer signal
1	2.052742	0.016217	0.012410	0.000744	0.000523
2	1.715995	0.012343	0.024751	0.001291	0.000617
3	2.046519	0.010661	0.014544	0.002208	0.000263
4	1.803944	0.010880	0.009416	0.001226	0.000309
5	1.682126	0.014349	0.010175	0.001302	0.000346
6	1.828368	0.011147	0.010376	0.000625	0.000508

Figure 12 shows the correct rate of six working conditions when the anchor point is 1.12.

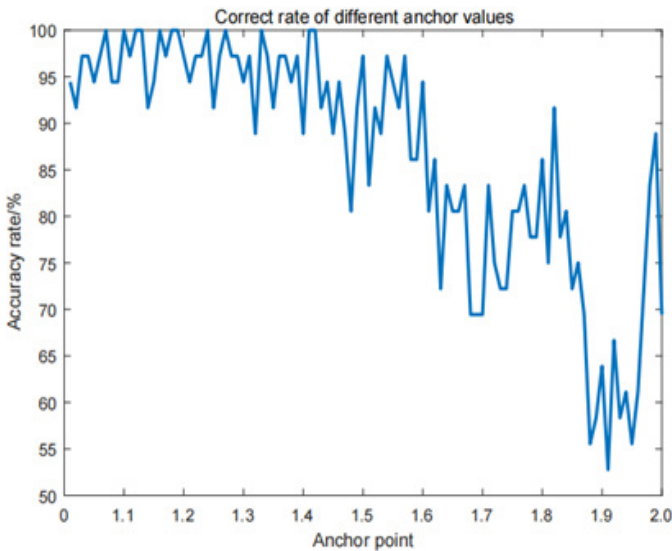


**Figure 12:** Different anchor values.

When the anchor point is 1.12, the anchor fitting values of six working conditions are shown in Table 7. In order to observe the discrimination of fault characteristics, the calculation results also selected different experimental data and repeated six experiments.

**Table 7:** Anchor fitting values.

	1	2	3	4	5	6
Normal	0.17906	0.11611	0.11688	0.18382	0.16234	0.16023
Inner1	2.32902	2.43770	2.48723	2.76815	2.67721	2.56609
Ball	1.75285	1.59300	1.71560	1.71282	1.74947	1.65654
Outer1	7.01223	7.13685	3.91041	7.50998	4.84612	6.32820
Inner2	13.36678	9.54820	12.98954	11.36724	16.89402	12.05624
Outer2	1.21601	1.31985	1.16045	1.39150	1.29891	1.15541

The results show that there is almost no intersection between the fitting values of anchor points corresponding to the six working conditions, which can be used as features for fault diagnosis. After many experiments, the range of anchor fitting values can be obtained. The fitting numerical range of anchor point in normal working conditions is 0.08644~0.13987. The fitting numerical range of fault 1 anchor point is 1.93677~3.01581.

The fitting numerical range of anchor point of rolling body fault in normal working condition is 1.22515~2.41464. The fitting numerical range of anchor point of outer ring fault 1 under normal working condition is 2.50308~13.14295. The fitting numerical range of fault 2 anchor point is 4.39316~29.52875. The fitting numerical range of anchor point of outer ring fault 2 under normal working condition is 1.03532~1.74344. After the range of anchor fitting value is determined, it can be used to distinguish six working conditions. This result is correct when the fitting values of anchor points in six working conditions are within the corresponding range. If the anchor fitting value is not in the corresponding range, the result will be wrong.

The diagnostic accuracy is obtained by classifying six working conditions by the extreme learning machine classifier. The fitting values of anchor points are used as features, which are divided into two groups of data: training and testing and input into the ELM classification model for training and testing. The first category represents normal conditions, the second category represents inner ring fault 1, the third category represents ball fault outer ring fault, the fourth category represents outer ring fault, the fifth category represents inner ring fault 2, and the sixth category represents outer ring fault 2. The anchor fitting value is used as the feature of training and testing data. There are 15 groups of training data in each working condition, 90 groups in 6 working conditions, and then 6 groups of testing data in each working condition, 36 groups in 6 working conditions. The fitting values of training data anchor points are shown in Table 8, and the fitting values of test data anchor points are shown in Table 9.

**Table 8:** Anchor fitting value of training data.

	normal working condition	inner ring fault 1	ball fault	outer ring fault 1	inner ring fault 2	outer ring fault 2
1	0.181393	2.618817	1.712822	4.629568	13.094801	1.489802
2	0.127293	2.753595	1.593002	8.027482	17.449723	1.279488
3	0.120234	2.333917	1.752850	3.910408	11.556697	1.216012
4	0.162344	2.329024	1.826760	5.854089	15.144390	1.391501
5	0.133126	2.437697	1.933177	6.328197	13.366781	1.314201
6	0.116876	2.677208	2.310330	4.846123	12.989539	1.460101
7	0.179062	2.631017	1.604479	5.003566	15.276742	1.484300
8	0.160229	2.372211	1.616120	7.136850	9.548197	1.584440
9	0.183816	2.384859	1.595506	4.743769	12.056239	1.196855
10	0.116105	2.449524	1.673202	7.012235	19.717810	1.410062
11	0.124492	2.105284	1.656535	5.226698	11.367244	1.268277
12	0.159628	2.141258	1.593521	6.058408	10.567740	1.298909
13	0.126925	2.572458	1.649264	5.318240	12.597680	1.245198
14	0.121454	2.768154	1.571686	9.025844	14.550618	1.360676
15	0.119055	2.487228	1.625889	7.509978	11.435785	1.170739

The ordinate of Figure 13 and Figure 14 shows the working state types of rolling bearings, 1 represents normal working state, 2 represents inner ring failure 1, 3 represents ball failure, 4 represents outer ring failure, 5 represents inner ring failure 2, and 6 represents outer ring failure 2. The red circle indicates the predicted value obtained after ELM calculation, and the blue circle indicates the real value corresponding to the working condition classification. As shown in Figure 13 and Figure 14, the extreme learning machine classifier classifies the normal working conditions and five fault working conditions, and the fault diagnosis accuracy rate characterized by the anchor fitting value reaches 97.2%, shows that six working conditions of rolling bearings can be diagnosed with high accuracy.

**Table 9:** Anchor fitting value of test data.

	normal working condition	inner ring fault 1	ball fault	outer ring fault 1	inner ring fault 2	outer ring fault 2
1	0.127456	2.437928	1.705957	4.335145	11.366106	1.319846
2	0.133194	2.388908	1.749469	5.083932	10.622493	1.302657
3	0.086439	2.476930	1.694581	5.746420	16.894021	1.576876
4	0.146722	2.476000	1.647039	5.660225	12.348784	1.449702
5	0.107368	2.073945	1.715604	6.151780	15.444343	1.443867
6	0.188838	2.566092	1.555072	4.154749	13.624653	1.340219

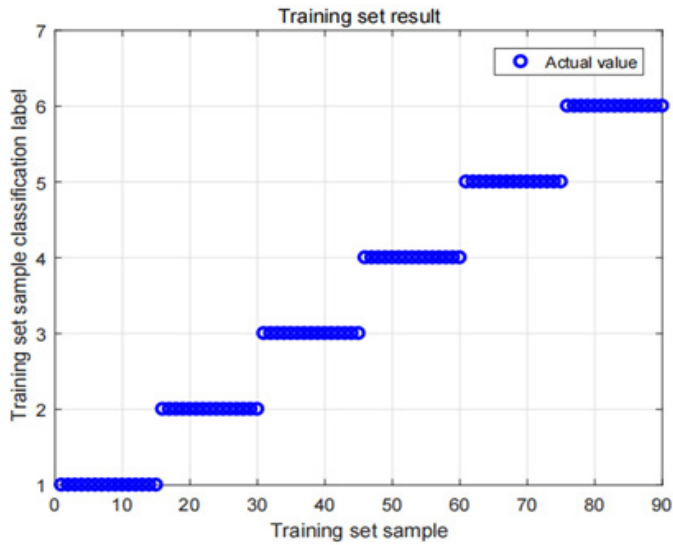


**Figure 13:** Training set prediction results comparison.

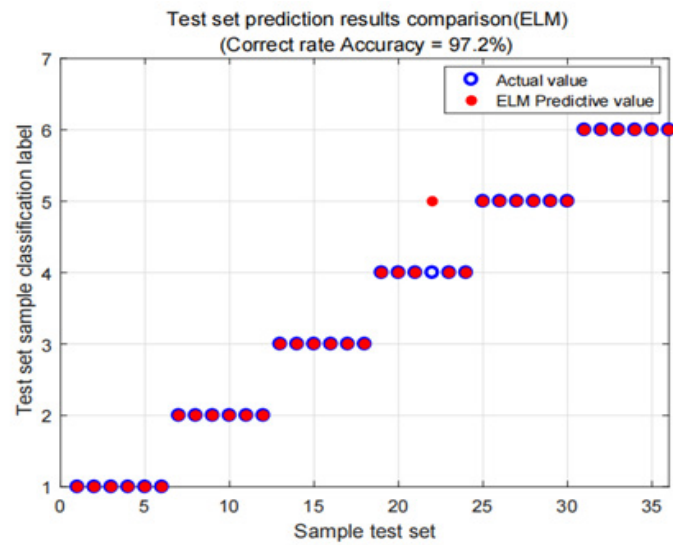


**Figure 14:** Test set prediction results comparison.

### Comparative Experiments

#### Comparative Experiments 1: with different moment orders'

Compared with the present method under different moment orders. The accuracy of the first-order method combined with EEMD decomposition is 23.1%. The accuracy of the second-order method combined with EEMD decomposition is 73.9%. The accuracy of the third-order method combined with EEMD decomposition is 34.4%. The accuracy of the present method is 97.5%. The four methods were repeated ten times, respectively. Table 10 to Table 12 show the anchor fitting values of comparative experiments with different moments. Table 13 shows the accuracy rate and average results of the comparative experiment with different moment orders.

**Table 10:** Anchor fitting value of Pseudo-first moment.

	normal working condition	inner ring fault 1	ball fault	outer ring fault 1	inner ring fault 2	outer ring fault 2
1	0.007543	-0.001360	0.002008	0.002980	0.003490	0.004103
2	0.010479	0.000021	-0.001080	-0.003122	0.003409	0.001099
3	0.002963	0.001462	-0.001350	0.003798	-0.001181	0.007930
4	0.005594	0.002306	0.003530	-0.001087	0.002352	0.008704
5	0.017195	0.000316	0.002450	-0.002431	0.003575	0.012723
6	0.002016	0.003223	0.002789	-0.004244	-0.000058	0.001178
7	0.001813	0.001493	0.001239	-0.006478	0.002546	-0.000078
8	0.003528	-0.007616	0.006131	0.004363	0.003654	0.007224
9	0.009527	0.003084	-0.000907	-0.004744	-0.000946	0.003825
10	0.001865	-0.004106	-0.002806	0.004150	0.001946	-0.010844
11	0.000620	0.001388	-0.004992	0.000537	-0.005889	0.002843
12	0.003786	0.005720	0.001116	0.002670	0.004863	-0.008482
13	0.006115	0.002950	0.002457	0.003284	0.000881	-0.008684
14	0.009396	0.002598	-0.003275	-0.003303	0.005532	0.003612
15	0.009726	0.005209	-0.000336	-0.000795	0.001777	0.002643

**Table 11:** Anchor fitting value of Pseudo-second moment.

	normal working condition	inner ring fault 1	ball fault	outer ring fault 1	inner ring fault 2	outer ring fault 2
1	0.274508	0.633283	0.724123	0.758212	0.741464	0.666049
2	0.218524	0.650297	0.729518	0.751612	0.713334	0.650795
3	0.233791	0.654194	0.716410	0.754879	0.743892	0.653807
4	0.256025	0.645989	0.738111	0.758338	0.680909	0.661458
5	0.255557	0.643043	0.723870	0.753258	0.751570	0.686035
6	0.276423	0.633080	0.726484	0.755179	0.720359	0.707747
7	0.243140	0.646026	0.724277	0.757112	0.708792	0.663230
8	0.228540	0.635356	0.728024	0.761926	0.739021	0.657754
9	0.253539	0.643018	0.729871	0.758508	0.707766	0.677805
10	0.229966	0.645415	0.722012	0.754723	0.725420	0.687437
11	0.262691	0.655338	0.733514	0.756410	0.684090	0.676742
12	0.202618	0.640378	0.731545	0.749055	0.732881	0.675362
13	0.231968	0.625888	0.719490	0.764066	0.732643	0.686062
14	0.255965	0.663411	0.729928	0.760096	0.686804	0.650805
15	0.207113	0.642403	0.734648	0.742157	0.727847	0.680840

**Table 12:** Anchor fitting value of Pseudo-third moment.

	normal working condition	inner ring fault 1	ball fault	outer ring fault 1	inner ring fault 2	outer ring fault 2
1	0.002101	0.013924	0.015753	0.005557	0.081769	0.001763
2	0.002194	-0.006306	-0.003695	-0.039241	0.034552	0.028026
3	-0.000493	-0.001825	0.004415	0.065029	0.059250	-0.009743
4	-0.000813	0.010431	0.003497	-0.073414	0.039217	-0.006175
5	0.005126	0.005859	0.001341	-0.016959	0.077821	0.006805
6	-0.001002	0.014557	-0.008915	-0.008516	-0.032816	-0.001190
7	-0.000318	0.016641	-0.000386	-0.013561	0.061884	-0.011250
8	-0.001226	-0.009072	0.003154	0.059697	0.019967	0.005780
9	0.000665	0.030147	-0.002965	0.018134	-0.018703	-0.009082
10	0.000102	0.008358	0.001005	0.024589	-0.050546	-0.003335
11	-0.007411	0.005427	-0.000966	0.007183	-0.019743	0.007837
12	-0.002883	0.005086	0.007147	0.028310	-0.037787	0.012822
13	-0.002000	0.027242	-0.014193	0.014589	0.002512	-0.016529
14	0.001100	0.003196	-0.003758	-0.011354	0.103346	-0.010513
15	0.002598	0.005234	0.013833	-0.009947	0.045571	0.001002

**Table 13:** Comparative results with different moment order.

	Pseudo-first moment EEMD	Pseudo-second moment EEMD	Pseudo-third moment EEMD	Present method
1	25.0%	75.0%	36.1%	100.0%
2	22.2%	72.2%	36.1%	97.2%
3	19.4%	69.4%	38.9%	94.4%
4	27.8%	75.0%	30.6%	100.0%
5	19.4%	77.8%	30.6%	94.4%
6	16.7%	69.4%	30.6%	97.2%
7	27.8%	75.0%	47.2%	100.0%
8	25.0%	72.2%	33.3%	97.2%
9	16.7%	75.0%	30.6%	100.0%
10	30.6%	77.8%	30.6%	94.4%
Mean value	23.1%	73.9%	34.4%	97.5%

From Table 10 to Table 12, it can be seen that the pseudo first moment, pseudo second moment and pseudo third moment are quite unstable. Among them, the pseudo first-order moment and pseudo third-order moment still have the problem of positive and negative transformation, which greatly increases the instability of interpolation fitting. The results show that the accuracy of this method improves by 77.4% compared with the first-order method, 23.6% compared with the second-order method, and 63.1% compared with the third-order method.

### Comparative Experiments 2: with different decomposition methods

Through the standardized processing of data, the original data can be converted into Compared with the present method under different decomposition conditions. The accuracy of EMD decomposition method is 78.0%. The accuracy of VMD decomposition method is 91.7%. The accuracy of this method is 97.5%. The three methods were repeated ten times, respectively. Table 14 and Table 15 show the anchor fitting values of comparative experiments of different decomposition methods. Table 16 shows the accuracy rate and average results of the experiment.

As can be seen from Table 14 and Table 15, neither EMD nor VMD can achieve good results. There is a serious cross between the data, which can not be used as a feature to identify different working conditions. Moreover, EMD still has the problem of modal aliasing, which greatly reduces the accuracy of final identification. The results show that the present method improves the decomposition accuracy by 19.5% compared with EMD decomposition and 5.8% compared with VMD decomposition.

### Comparative Experiments 3: with original pseudo fourth-order moment [8]

In order to further prove the effectiveness of the present method, comparative experiments with the original pseudo-fourth-order moment method is carried out, which is published in reference [8]. The specific improvement for original PFOM includes that two fault diagnosis conditions are added, and the accuracy rate is improved. The accuracy of the original pseudo fourth-order moment method is 95.4%. The accuracy of the present method is 97.5%, which is 2.1% higher than the original pseudo fourth-order moment method. The two methods were

repeated ten times, respectively. Table 17 shows the accuracy rate and average results of the experiment.

**Table 14:** Anchor fitting value of EMD.

	normal working condition	inner ring fault 1	ball fault	outer ring fault 1	inner ring fault 2	outer ring fault 2
1	0.00646	0.05676	0.23212	0.47127	-0.32622	0.27607
2	-0.00188	0.08461	0.27881	0.58396	0.07616	0.27077
3	-0.00108	0.08414	0.17973	0.46986	-0.30306	0.22566
4	0.00327	0.06534	0.25797	0.47516	-0.06078	0.21426
5	0.00110	0.04853	0.20524	0.55024	-0.27453	0.25071
6	-0.00039	0.12705	0.24049	0.54036	-0.43171	0.22276
7	0.00677	0.08950	0.29530	0.58164	-0.18189	0.17577
8	0.00647	0.11822	0.24661	0.49345	-0.51515	0.18451
9	0.00675	0.03911	0.24257	0.44054	-0.04672	0.13823
10	0.00588	0.10688	0.28570	0.55702	-0.29173	0.21825
11	-0.00116	0.01209	0.24644	0.53362	-0.12283	0.19742
12	0.00214	0.06370	0.23617	0.57911	-0.38788	0.23394
13	0.00981	0.05540	0.19223	0.46450	-0.22017	0.21928
14	0.01743	0.03287	0.30427	0.45405	-0.21252	0.20886
15	0.02009	0.06659	0.18442	0.46718	-0.40922	0.20747

**Table 15:** Anchor fitting value of VMD.

	normal working condition	inner ring fault 1	ball fault	outer ring fault 1	inner ring fault 2	outer ring fault 2
1	0.00646	0.05676	0.23212	0.47127	-0.32622	0.27607
2	-0.00188	0.08461	0.27881	0.58396	0.07616	0.27077
3	-0.00108	0.08414	0.17973	0.46986	-0.30306	0.22566
4	0.00327	0.06534	0.25797	0.47516	-0.06078	0.21426
5	0.00110	0.04853	0.20524	0.55024	-0.27453	0.25071
6	-0.00039	0.12705	0.24049	0.54036	-0.43171	0.22276
7	0.00677	0.08950	0.29530	0.58164	-0.18189	0.17577
8	0.00647	0.11822	0.24661	0.49345	-0.51515	0.18451
9	0.00675	0.03911	0.24257	0.44054	-0.04672	0.13823
10	0.00588	0.10688	0.28570	0.55702	-0.29173	0.21825
11	-0.00116	0.01209	0.24644	0.53362	-0.12283	0.19742
12	0.00214	0.06370	0.23617	0.57911	-0.38788	0.23394
13	0.00981	0.05540	0.19223	0.46450	-0.22017	0.21928
14	0.01743	0.03287	0.30427	0.45405	-0.21252	0.20886
15	0.02009	0.06659	0.18442	0.46718	-0.40922	0.20747

**Table 16:** Comparative results with different decomposition methods.

	Pseudo-first moment EEMD	Pseudo-second moment EEMD	Pseudo-third moment EEMD	Present method
1	76.7%	96.7%	100.0%	100.0%
2	83.3%	93.3%	97.2%	97.2%
3	70.0%	86.7%	94.4%	94.4%
4	76.7%	93.3%	100.0%	100.0%
5	90.0%	96.7%	94.4%	94.4%
6	83.3%	86.7%	97.2%	97.2%
7	70.0%	90.0%	100.0%	100.0%
8	80.0%	93.3%	97.2%	97.2%
9	76.7%	86.7%	100.0%	100.0%
10	73.3%	93.3%	94.4%	94.4%
Mean value	78.0%	91.7%	97.5%	97.5%

**Table 17:** Comparative results with original pseudo fourth-order moment.

	Original pseudo fourth-order moment	Present method
1	95.8%	100.0%
2	91.7%	97.2%
3	100.0%	94.4%
4	91.7%	100.0%
5	95.8%	94.4%
6	87.5%	97.2%
7	100.0%	100.0%
8	95.8%	97.2%
9	100.0%	100.0%
10	95.8%	94.4%
Mean value	95.4%	97.5%

## Conclusion

Aiming at the fault diagnosis of rolling bearings, a new feature extraction method based on EEMD and improved PFOM is proposed. In the application of PFOM, it is innovatively associated with interpolation fitting. The concept of anchor point was first put forward. By introducing the anchor point into the fitting curve, the fitting value of the anchor point is regarded as the fault feature of the rolling bearing. This improvement greatly expands the application of pseudo four moments in fault diagnosis. In the final test, the average accuracy of classification by ELM reached 97.5%. The feasibility of this method is proved, and it can diagnose six working conditions of rolling bearings with high accuracy. This innovation has opened up new ideas for researchers in the field of fault diagnosis and played a certain role in promoting the development of the field.

## References

- Sun, Y., Li, S., Wang, Y., et al. (2021). Fault diagnosis of rolling bearing based on empirical mode decomposition and improved manhattan distance in symmetrized dot pattern image. *Mechanical Systems and Signal Processing*, 159, 107817. <https://doi.org/10.1016/j.ymssp.2021.107817>
- Xu, Y., Zhang, K., Ma, C., et al. (2019). Adaptive Kurtogram and its applications in rolling bearing fault diagnosis. *Mechanical Systems and Signal Processing*, 130, 87-107. <https://doi.org/10.1016/j.ymssp.2019.05.003>
- Lin, H., Wu, F., & He, G. (2020). Rolling bearing fault diagnosis using impulse feature enhancement and nonconvex regularization. *Mechanical Systems and Signal Processing*, 142, 106790. <https://doi.org/10.1016/j.ymssp.2020.106790>
- Cerrada, M., Snchez, R. V., Li, C., et al. (2018). A review on data-driven fault severity assessment in rolling bearings. *Mechanical Systems and Signal Processing*, 99, 169-196. <https://doi.org/10.1016/j.ymssp.2017.06.012>
- Cao, H., Niu, L., Xi, S., et al. (2018). Mechanical model development of rolling bearing-rotor systems: A review. *Mechanical Systems and Signal Processing*, 2018, 102: 37-58. <https://doi.org/10.1016/j.ymssp.2017.09.023>
- Li, J., Zhang, J., Li, M., et al. (2019). A novel adaptive stochastic resonance method based on coupled bistable systems and its application in rolling bearing fault diagnosis. *Mechanical Systems and Signal Processing*, 114, 128-145. <https://doi.org/10.1016/j.ymssp.2018.05.004>
- Chen, B., Shen, B., Chen, F., et al. (2019). Fault diagnosis method based on integration of RSSD and wavelet transform to rolling bearing. *Measurement*, 131, 400-411. <https://doi.org/10.1016/j.measurement.2018.07.043>
- Sun, Y., Xu, B., & Wang, X. (2021). Pseudo fourth-order moment based bearing fault feature reconstruction and diagnosis. *ISA transactions*, 118, 238-246. <https://doi.org/10.1016/j.isatra.2021.02.005>
- Sun, Y., Li, S., & Wang, X. (2021). Bearing fault diagnosis based on EMD and improved Chebyshev distance in SDP image. *Measurement*, 176, 109100. <https://doi.org/10.1016/j.measurement.2021.109100>
- Li, X., Ma, Z., Kang, D., et al. (2020). Fault diagnosis for rolling bearing based on VMD-FRFT. *Measurement*, 155, 107554. <https://doi.org/10.1016/j.measurement.2020.107554>
- Han, T., Liu, Q., & Zhang, L., et al. (2019). Fault feature extraction of low speed roller bearing based on Teager energy operator and CEEMD. *Measurement*, 138, 400-408. <https://doi.org/10.1016/j.measurement.2019.02.053>
- Pang, B., Nazari, M., & Tang, G. (2022). Recursive variational mode extraction and its application in rolling bearing fault diagnosis. *Mechanical Systems and Signal Processing*, 165, 108321. <https://doi.org/10.1016/j.ymssp.2021.108321>
- Li, X., Zhang, W., & Ding, Q. (2019). Understanding and improving deep learning-based rolling bearing fault diagnosis with attention mechanism. *Signal processing*, 161, 136-154. <https://doi.org/10.1016/j.sigpro.2019.03.019>
- Xu, Y., Deng, Y., Ma, C., et al. (2021). The Enfigram: A robust method for extracting repetitive transients in rolling bearing fault diagnosis. *Mechanical Systems and Signal Processing*, 158, 107779. <https://doi.org/10.1016/j.ymssp.2021.107779>
- Li, X., Yang, Y., Pan, H., et al. (2020). Non-parallel least squares support matrix machine for rolling bearing fault diagnosis. *Mechanism and Machine Theory*, 145, 103676. <https://doi.org/10.1016/j.mechmachtheory.2019.103676>
- Hoang, D. T., Kang, H. J. (2019). A survey on deep learning based bearing fault diagnosis. *Neurocomputing*, 335, 327-335. <https://doi.org/10.1016/j.neucom.2018.06.078>
- Zheng, J., Pan, H., Yang, S., et al. (2018). Generalized composite multiscale permutation entropy and Laplacian score based rolling bearing fault diagnosis. *Mechanical Systems and Signal Processing*, 99, 229-243. <https://doi.org/10.1016/j.ymssp.2017.06.011>
- Pang, S., Yang, X., Zhang, X., et al. (2021). Fault diagnosis of rotating machinery components with deep ELM ensemble induced by real-valued output-based diversity metric. *Mechanical Systems and Signal Processing*, 159, 107821. <https://doi.org/10.1016/j.ymssp.2021.107821>
- Hou, F., Chen, J., & Dong, G. (2018). Weak fault feature extraction of rolling bearings based on globally optimized sparse coding and approximate SVD. *Mechanical Systems and Signal Processing*, 111, 234-250. <https://doi.org/10.1016/j.ymssp.2018.04.003>
- Huang, C., Huang, H., Li, Y., et al. (2021). A novel deep convolutional neural network-bootstrap integrated method for RUL prediction of rolling bearing. *Journal of Manufacturing Systems*, 61, 757- 772. <https://doi.org/10.1016/j.jmsy.2021.03.012>
- Li, X., Jiang, H., Wang, R., et al. (2021). Rolling bearing fault diagnosis using optimal ensemble deep transfer network. *Knowledge-Based Systems*, 213, 106695. <https://doi.org/10.1016/j.knosys.2020.106695>
- Zhao, B., Zhang, X., Li, H., et al. (2020). Intelligent fault diagnosis of rolling bearings based on normalized CNN considering data imbalance and variable working conditions. *Knowledge-Based Systems*, 199, 105971. <https://doi.org/10.1016/j.knosys.2020.105971>
- Li, H., Liu, T., Wu, X., et al. (2019). Application of EEMD and improved frequency band entropy in bearing fault feature extraction. *ISA transactions*, 88, 170-185. <https://doi.org/10.1016/j.isatra.2018.12.002>

24. Zheng, K., Luo, J., Zhang, Y., et al. (2019). Incipient fault detection of rolling bearing using maximum autocorrelation impulse harmonic to noise deconvolution and parameter optimized fast EEMD. *ISA transactions*, 89, 256-271. <https://doi.org/10.1016/j.isatra.2018.12.020>
25. He, C., Wu, T., Gu, R., et al. (2021). Rolling bearing fault diagnosis based on composite multiscale permutation entropy and reverse cognitive fruit fly optimization algorithm Cextreme learning machine. *Measurement*, 173, 108636. <https://doi.org/10.1016/j.measurement.2020.108636>